https://doi.org/10.5194/egusphere-2026-4836
Preprint. Discussion started: 24 August 2026

Winter Jet Stream Clustering over Australia and its Role in Extreme Precipitation Events

Anna Kuhn[1,2], Chenhui Jin[2,3], Elizabeth Ritchie[2,3], and Michael Sprenger[1]

[1]Institute for Atmospheric and Climate Science, ETH Zurich, Switzerland
[2]Australian Research Council Centre of Excellence for the Weather of the 21st Century, VIC Australia
[3]School of Earth, Atmosphere and Environment, Monash University, VIC Australia

Correspondence: Anna Kuhn (anna.kuhn@usys.ethz.ch)

Abstract. Jet streams substantially affect the surface weather, including extreme events. Even small changes in the position and strength of the jet stream can have a substantial impact on weather systems, and thus recent studies have linked many extreme weather events to the characteristics of the jet stream. Therefore, it is important to better understand the variability of the jet stream and how it specifically and mechanistically affects surface weather. Despite this importance, there is limited research on jet stream variability in the Southern Hemisphere. In this study, we explore the variability of the wintertime jet stream over Australia by applying a K-means clustering approach to vertically-averaged wind speed fields. Five jet stream configurations are defined, and it is shown that the wintertime jet stream over Australia exhibits substantial variability, particularly in the longitudinal location of the wind speed maximum. The clustering approach enables us to analyze patterns of upper-level forced vertical motion for the five jet configurations and how precipitation is related to these patterns. The strongest ascent occurs just south of the jet maximum, coinciding with anomalously wet regions. Furthermore, we define extreme precipitation events as those exceeding the 99.5$^{\text{th}}$ percentile for Adelaide, Brisbane, Hobart, Melbourne, Perth, and Sydney using precipitation data from the Australian Gridded Climate Data (AGCD). In each of these capital cities, a higher percentage of extreme precipitation events is associated with one or two of the jet configurations, and in most of the cities, these events are linked to increased upper-level forced upward motion in the vicinity of the jet stream aloft. Extreme precipitation events are often associated with either a particularly strong jet stream acting as a waveguide for surface weather systems or a weaker jet stream disturbing the upper-level waveguide and leading to potential vorticity streamers, which have recently been linked to heavy precipitation events.

1 Introduction

Jet streams are narrow bands of westerly winds in the upper troposphere that can be found in the midlatitudes of both hemispheres (e.g., Koch et al., 2006). They are an important feature of the large-scale atmospheric circulation, because they substantially influence day-to-day weather changes (e.g., Spensberger et al., 2020), are often a prerequisite for extratropical cyclogenesis (e.g., Lorenz, 1955; Trenberth, 1991), and can be related to various extreme weather events (e.g., Li et al., 2024; Seager et al., 2010). The upper-level jet can be divided into the subtropical jet (STJ) and the eddy-driven jet (EDJ) depending on the location and mechanism of formation (e.g., Spensberger and Spengler, 2020). The STJ, also referred to as a shallow jet

https://doi.org/10.5194/egusphere-2026-4836
Preprint. Discussion started: 24 August 2026

(Koch et al., 2006), is located in the subtropics at the upper edge of the Hadley cell and forms due to the conservation of angular momentum (e.g., Krishnamurti, 1961; Held and Hou, 1980). The EDJ is located further polewards in the region of strong baroclinicity and forms due to the convergence of eddy-momentum flux (e.g., Palmén, 1948; Hoskins et al., 1983). It is also referred to as a deep jet, due to its larger vertical extent (Koch et al., 2006). Koch et al. (2006) detects jets as distinct objects in space and time, while Spensberger and Spengler (2020) and Bösiger et al. (2022) detect them as jet axes. Both methods allow analysis for the spatial distribution, intra-seasonal variability and distinction of the two jet types in a time-mean perspective.

The distribution and intensity of the jet streams differ between seasons and hemispheres (e.g., Koch et al., 2006) and in practice, it is often difficult to clearly distinguish between them (e.g., Lee and Kim, 2003; Li and Wettstein, 2012). From a climatological perspective, a double-jet structure can be observed throughout most of the Southern Hemisphere (Spensberger and Spengler, 2020). The strongest jet stream is found in the austral winter (JJA) with a strong STJ located over Australia extending from the Indian Ocean to the Pacific Ocean. In austral summer (DJF), the jet stream becomes weaker and shifts polewards to higher latitudes, whereby it extends from the Atlantic Ocean to the South of Australia (Koch et al., 2006). Compared to the Northern Hemisphere, the jet stream in the Southern Hemisphere is more persistent throughout all seasons, primarily due to differences in land-sea distribution and topography between the two hemispheres (Spensberger and Spengler, 2020). Given Australia's subtropical location, the STJ is of particular interest for this region as it lies along the boundary between the tropics and the extratropics and thus plays an important role in tropical-extratropical interactions (Davidson et al., 2007; McKay et al., 2023).

On a daily to subseasonal time scale, the jet stream varies considerably in its structure, location and intensity compared to its climatological mean. Accordingly, changes in weather patterns in the midlatitudes are often associated with meridional shifts in the jet stream location (Woollings et al., 2018). Specifically, weaker jets typically coincide with increased latitudinal excursions, while stronger jets remain closer to their climatological position (Woollings et al., 2018). In the Northern Hemisphere, the STJ has generally been found to be less wavy than the EDJ, i.e., to exhibit less and weaker meridional excursions (Martin, 2021). Gillett et al. (2021) noted that the STJ exhibits only minor interannual variability in winter in the Indo-Pacific sector (70°E – 120°W), with a deviation of approximately 5% in its intensity and a latitude shift of less than 1°. On the east coast of Australia, a weaker STJ generally leads to increased precipitation (Maher and Sherwood, 2016). The opposite has been found for the west coast of Australia, where a weakened STJ has been associated with reduced precipitation (Frederiksen and Frederiksen, 2007). It has also been noted that the STJ only influences precipitation in winter and spring (Maher and Sherwood, 2016). In contrast, Risbey et al. (2009) found that a stronger STJ coincides with increased precipitation in southeastern Australia, because cut-off low intensity increases due to a locally strengthened STJ. The large-scale variability of the atmospheric circulation produces fluctuations in synoptic and mesoscale weather systems, such as cyclones and fronts, which in turn affect precipitation (McKay et al., 2023). These findings highlight the importance of the jet stream, particularly with regard to winter precipitation. However, there are only a limited number of studies that have analyzed the role of the jet stream on precipitation in Australia, and there are conflicting results of the effect of a weaker or stronger STJ on precipitation.

On a global scale, an increasing number of studies are relating extreme weather events to jet variability (e.g., Seager et al., 2010; Ashcroft et al., 2009; Galfi and Messori, 2023), emphasizing the importance on both the synoptic and meso-scales.

https://doi.org/10.5194/egusphere-2026-4836
Preprint. Discussion started: 24 August 2026

Often, anomalous large-scale circulation patterns are directly related to temperature and/or precipitation extremes (Lehmann and Coumou, 2015). The majority of these studies consider extremes in the Northern Hemisphere, particularly in Europe and the North Atlantic region. In Europe, the highest frequencies of extreme events are observed during anomalously zonal or fast jet events or a combination of both. Specifically, the strongest connection is found between precipitation extremes and fast or merged jet configurations (Galfi and Messori, 2023). Several extreme weather events, such as the exceptionally hot summer of 2022 in Europe (Li et al., 2024) or the anomalously snowy winter of 2009/10 in North America and Europe (Seager et al., 2010) have been linked to jet stream anomalies. A study in Central Asia found an increase in precipitation downstream of a split-jet region (Gu et al., 2025), and merged states of the STJ and EDJ have been linked to cold events in an earlier study in Australia (Ashcroft et al., 2009), as well as to extreme precipitation in the Nashville Flood in 2010 (Winters and Martin, 2014). Suresan et al. (2025) found that the merging of jets is related to various extreme weather events in the Northern Hemisphere during winter, substantially impacting regional precipitation distribution by enhancing or suppressing precipitation locally. These findings demonstrate the importance of analyzing the variability of the jet stream at different locations and for different time scales, and highlight the complex and diverse relationships between the jet stream and its influence on surface weather.

Several previous studies have emphasized the importance of the ageostrophic circulation induced by jet streaks, i.e., wind maxima in the jet stream, for extreme weather events, such as tornadoes and strong winds (e.g., Rose et al., 2004; Clark et al., 2009), as well as for heavy precipitation events (Zhao et al., 2022). Jet streaks occur in regions with strong potential vorticity (PV) gradients (Bukenberger et al., 2023, 2025) and strong horizontal and vertical wind shear. They are also usually accompanied by ageostrophic circulations, which act on the geostrophic flow to restore the thermal wind balance by inducing vertical motion (Hoskins and James, 2014). This vertical forcing can be quantified using the quasi-geostrophic omega (QGω) equation (Davies, 2015; Davies et al., 2026). It has been used to analyze the impact of large-scale circulation on heavy precipitation (e.g., Zhao et al., 2022). In particular, the four-quadrant model (4Q model) conceptually describes the relationship between jet streaks and the forcing of vertical motion (Beebe and Bates, 1955). In the case of linear jet streaks, upward motion is expected to be forced at the equatorward entrance and poleward exit of the jet streak, and vice versa for downward motion. The regions and amplitude of vertical forcing change substantially with the curvature and orientation of the jet streaks (Keyser and Shapiro, 1986; Moore and Vanknowe, 1992). In summary, understanding vertical motion in the vicinity of the jet stream is important for identifying regions of (heavy) precipitation. To our knowledge, no previous work has demonstrated the distribution of vertical forcing in the vicinity of the jet stream from a climatological perspective and specifically over Australia, nor has it been considered for different jet configurations.

Different methods can be used to capture the variability of the jet stream. Common methods include the use of jet indices based on zonal mean winds (e.g., Woollings et al., 2018) or modes of climate variability, such as the North Atlantic Oscillation (NAO), the Pacific-North America pattern (PNA), or the southern annular mode (SAM) (e.g., Limpasuvan and Hartmann, 1999; Seager et al., 2010). The latter characterize the jet stream variability indirectly through the variability of geopotential or sea level pressure. Spensberger et al. (2020) showed that the expected relationship between the jet and major climate modes of variability does not apply to the Southern Hemisphere, where the SAM and the mean state of the jet interact in a more complex way. Considering the jet only as a zonal mean also turns out to be challenging when it comes to describing its spatial and

https://doi.org/10.5194/egusphere-2026-4836
Preprint. Discussion started: 24 August 2026

temporal variability, because significant deviations from the mean state occur, particularly during the winter months. These deviations are obscured by the zonal averaging (Arakelian and Codron, 2012). Additionally, Auestad et al. (2024) noted that other meteorological fields, such as vertical velocity and precipitation are highly sensitive to the orientation of the jet axis, which is – by definition – not considered in the zonal mean. Another key method for evaluating the variability of the jet stream involves clustering approaches applied to object-based jet identification (e.g., Koch et al., 2006; Spensberger and Spengler, 2020). For example, Banderier et al. (2025) combined these methodologies by applying clustering approaches to jet detection schemes to study the intra-seasonal variability of Euro-Atlantic jet streams during summer.

This study applies a similar approach to that described in Banderier et al. (2025) to capture the variability of the jet stream in the Australian region during austral winter by clustering the jet stream based on vertically-averaged wind speed fields. The selected methods enable us to systematically analyze different jet configurations and their deviations from climatology. Moreover, we study how jet configurations are reflected in their effects on the surface weather (precipitation). The main objectives of this study are to improve the understanding of the jet stream dynamics over Australia and to describe the jets' role in extreme precipitation events. Our work focuses on the jet stream in winter since this is the season when the jet stream is strongest, particularly the STJ, and when it occurs most frequently over the Australian continent. More specifically, we address the following questions:

1. What are the dominant jet stream configurations in the Australian region in winter, and how do they differ from the winter climatology?

2. What is the spatial distribution of precipitation and upper-level forced vertical motion associated with different jet stream configurations?

3. Are extreme precipitation events in major Australian cities linked to specific jet stream configurations, and what role does the jet stream play in these events in inducing vertical motion and/or governing (surface) weather systems?

4. How do days with extreme precipitation differ from other days within a given jet stream configuration in terms of dynamic drivers (e.g., forcing for vertical motion), moisture availability, and synoptic features?

This paper is structured as follows. The datasets and methods are described in section 2. Section 3 presents the results of the jet cluster analysis, while section 4 presents the results for extreme precipitation events. Section 5 then describes and discusses the role of the jet stream in extreme precipitation events. Finally, some concluding remarks are presented in section 6.

2 Data and Methods

2.1 Australian Gridded Climate Data

The Australian Gridded Climate Data (AGCD), the official climate analysis dataset of the Bureau of Meteorology (BoM), is derived from in situ observations (Jones et al., 2009) and provides daily and monthly data with a horizontal grid spacing of 0.05°. We use daily precipitation data representing the total precipitation accumulated over 24 hours from 09:00 local

https://doi.org/10.5194/egusphere-2026-4836
Preprint. Discussion started: 24 August 2026

time the previous day to 09:00 local time on the current day. The AGCD precipitation data are only available over land. For any analysis that includes precipitation over sea, we use the total precipitation from ERA5 reanalysis (described in section 2.2).

Extreme precipitation events are identified for six different cities: Adelaide, Brisbane, Hobart, Melbourne, Perth and Sydney. First, the daily precipitation is spatially averaged over a 4° x 4° latitude/longitude box (red boxes in Fig. 1) centred on each city for all winter days (JJA) of the period 1980 to 2022. For Hobart, the precipitation is averaged over a box centred on Tasmania, rather than on the city itself. Specifically, the extreme precipitation events are defined as the days on which the daily mean precipitation exceeds the 99.5th percentile in the respective box. For multi-day extremes (three and five days), we calculate the multi-day sums using a moving window and define the percentiles of the accumulated time series. To assign the extreme events to the jet stream clusters (as defined in Section 3.1), we calculate the percentage of extreme precipitation days per cluster. For the multi-day events, all days within an extreme event are considered EPDs (i.e., all five days of a 5-day extreme event are considered individually when assigning numbers of clusters).

2.2 ERA5

Meteorological fields are obtained from the ERA5 reanalysis data provided by the European Centre for Medium-Range Weather Forecasts (ECMWF) (Hersbach et al., 2020). This reanalysis product combines observations and short-term model simulations to provide information on atmospheric variables globally. It is available hourly with a grid spacing of 31 km (0.25° x 0.25°) (Hersbach et al., 2020; Bell et al., 2021). The main variables used in this study are the zonal and meridional winds between 400 and 100 hPa, the potential vorticity (PV) at 330 K, and the mean sea level pressure. Additionally, the vertical integral of the northward and eastward water vapour flux are combined to obtain the integrated vapour transport (IVT). Daily mean fields are obtained by averaging six-hourly data (00, 06, 12 and 18 UTC) for the winter months (JJA) from 1980 to 2022. For the daily precipitation, the total precipitation (TP) is accumulated over 24 hours from 00 to 23 UTC. Precipitation anomalies are then calculated as the deviation from the winter climatology (JJA).

2.3 Weather features

To identify the jet stream, we use the vertically-averaged horizontal wind speeds following Koch et al. (2006). The horizontal wind speed is calculated at the following pressure levels: 400, 300, 250, 200 and 100 hPa. Vertical averaging is applied to account for the variations in tropopause height associated with latitude (Koch et al., 2006). The weighted vertical mean is then calculated as follows,

$$VEL = (0.5 \cdot U_{400} + 0.75 \cdot U_{300} + 0.5 \cdot U_{250} + 0.75 \cdot U_{200} + 0.5 \cdot U_{100})/3 \quad (1)$$

where VEL is the vertically-averaged horizontal wind velocity, and the subscripts represent the respective pressure levels. Koch et al. (2006) uses the resulting wind speed field and a threshold of VEL > 30 m s^{-1} to identify the jet streams as weather objects. However, since we are also interested in the wind maxima in the jet stream, we will skip this final step and use the

https://doi.org/10.5194/egusphere-2026-4836
Preprint. Discussion started: 24 August 2026

wind speed fields for our analyses. To be consistent, we calculate the daily mean of the six-hourly data for the wind speed fields.

Following Hauser et al. (2020) and Jin et al. (2024, 2025) we identify Eulerian weather features as described by Sprenger et al. (2017), including surface cyclones, fronts, and PV streamers (manifesting Rossby wave breaking). Their frequencies are calculated using six-hourly data, representing the percentage of time that the respective weather feature is present at a location. Specifically, cyclones are defined as sea level pressure minima and are limited by their outermost closed isobar (Wernli and Schwierz, 2006; Sprenger et al., 2017); fronts are detected as areas where the horizontal gradient of equivalent potential temperature at 700 hPa is greater than 4 K $(100\,\text{km})^{-1}$ (Jenkner et al., 2010; Schemm et al., 2015); and PV streamers are defined as filaments of stratospheric air on the 330 K isentropic surface using the -2 PVU contour (Wernli and Sprenger, 2007), whereby the filaments must meet specific length and width requirements (see Wernli and Sprenger, 2007, and Sprenger et al., 2017, for more details).

To quantify the forcing of vertical motion ω, we use quasi-geostrophic omega ($QG\omega$) (Davies, 2015; Davies et al., 2026), which is calculated using the $QG\omega$ equation as in Besson et al. (2021) and Reinert (2009). The Q-vector form of the $QG\omega$ equation is

$$(\sigma\nabla^2 + f_0^2\frac{\partial^2}{\partial p^2})\omega = -2\nabla\cdot\boldsymbol{Q} \tag{2}$$

with

$$\sigma(p) = -\frac{p}{R}\frac{T_v}{\theta}\frac{d\theta}{dp}, \tag{3}$$

where σ is the static stability in pressure coordinates, f_0 is the Coriolis parameter, R is the gas constant, T_v is the virtual temperature and θ is the potential temperature. The horizontal mean of the static stability is used following Besson et al. (2021).

The Q-vector is given by

$$\boldsymbol{Q} = \begin{pmatrix} \frac{\partial \boldsymbol{V_g}}{\partial x}\cdot\nabla\frac{\partial\phi}{\partial p} \\ \frac{\partial \boldsymbol{V_g}}{\partial y}\cdot\nabla\frac{\partial\phi}{\partial p} \end{pmatrix}, \tag{4}$$

where $\boldsymbol{V_g}$ is the geostrophic wind and ϕ is the geopotential. Eq. 2 suggests that the Q-vector convergence is associated with upward motion ($\omega < 0$) and Q-vector divergence with downward motion ($\omega > 0$) (Hoskins and James, 2014).

We partition the divergence of the Q-vector into upper-level forcing (above 550 hPa) and lower-level forcing (below 550 hPa) by setting the forcing term in Eq.2 to zero in the lower and upper parts, respectively. Consequently, the vertical motion at any level can be divided into that forced by upper-level features (e.g., jet) and lower-level features (e.g., front). Because we are primarily interested in the forcing caused by jet streams, the focus will be on the upper-level forcing. Furthermore, we consider positive and negative $QG\omega$ values separately to avoid cancellation of upward and downward forcing while compiling $QG\omega$ climatologies. Hence, negative (positive) $QG\omega$ values only are used to calculate the mean forcing of upward (downward) motion. Further details on the $QG\omega$ calculation can be found in (Reinert, 2009).

https://doi.org/10.5194/egusphere-2026-4836
Preprint. Discussion started: 24 August 2026

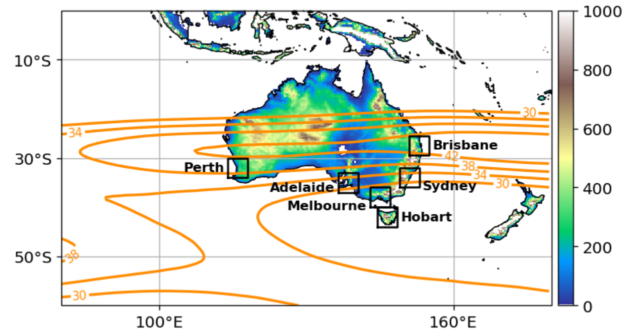

Figure 1. Climatology of the wintertime jet stream in the Australian region. The shading shows the topography in metres above mean sea level (masl). The orange contours show the vertically-averaged wind speeds between 400 and 100 hPa for the winter months (JJA) in m s^{-1}. The black boxes indicate the regions used to define the extreme precipitation events for the different capital cities (see section 4).

3 Jet stream configurations

First, we examine the jet stream climatology for the winter season (JJA) in the Australian sector. The mean of the vertically-averaged wind speeds is displayed in Fig. 1. A strong STJ lies over the Pacific, extending across the Australian continent at around 30°S, with the strongest winds mainly over and to the east of the continent. The EDJ is located between 50 and 60°S and exhibits weaker winds, with the wind maximum in the Indian Ocean shifted towards the southwest of Australia. The two climatological jets are clearly separated, with the STJ being stronger than the EDJ. However, this could also be due to the fact that the STJ is more stationary, while the EDJ is subject to greater fluctuations over time (Martin, 2021), which might result in weaker signals when averaging over time.

The climatology of the jet frequencies for each season can be found in Fig. S1 of the supplementary material. A double-jet structure is present in each season except for summer (Fig. S1). The mean distribution of the EDJ remains consistent throughout the year, whereas the STJ exhibits the highest frequencies in winter and lower frequencies in spring and autumn. This is consistent with the findings of previous studies (Koch et al., 2006; Spensberger and Spengler, 2020; Gillett et al., 2021), which also found the strongest jet in the Australian sector during winter and reported similar seasonal patterns and double-jet structures. Spensberger and Spengler (2020) also noted that a weak STJ is present on the Australian continent even in summer. Our results are most similar to Koch et al. (2006), which used the same method but with ERA-15 (Gibson et al., 1997).

3.1 Identification and characteristics of the jet configurations

To analyze the variability of the wintertime jet stream, we performed a K-means clustering on all winter days between 1980 and 2022. The method is proposed by Hartigan and Wong (1979), and groups the input data into a predefined number (K) of clusters. The patterns within a cluster should therefore be as similar as possible, while those between clusters should be as different as possible. The clustering is based on the vertically-averaged horizontal wind speeds (see section 2.3) over the domain from 80°- 180°E and 0°- 60°S (as shown in Fig. 1). This input data is the daily mean of the six-hourly data (00, 06,

https://doi.org/10.5194/egusphere-2026-4836
Preprint. Discussion started: 24 August 2026

12, 18 UTC) for all winter days. A challenge of clustering is to find an appropriate value for K. The optimal K should allow for enough clusters to capture the jet variability, while keeping the number of clusters as low as possible to avoid a high cluster similarity. We tested different values of K between 4 and 20 and calculated the Davies-Bouldin score for each case respectively (Davies and Bouldin, 1979). The score reaches its first local minimum at K = 5. Therefore, we chose K = 5 as the optimal number of clusters, and thus five main jet stream configurations are further considered for the winter months. We also repeated the clustering process by altering the domain sizes (not shown) and found that the clustering patterns resulting from K = 5 are insensitive to the choice of domain size.

The percentage of days in each cluster is similar: C3 and C4 each account for 22.4% of the days, followed by C5 with 20.7% of the days, and then C1 and C2 with 17.3% and 17.2%. Although the mean number of days in each cluster is similar for the period 1980-2022, there is a large interannual variability, with some clusters occurring more frequently in some years than in others. We compared the percentage of days in each cluster in the first 20 years of the study period (1981-2000) with the second 20 years (2001-2020; Fig. 2). Overall, the spread within a period is much greater than the difference in medians between the earlier and later period. C4 has the highest spread of values ranging from 0% to almost 50% of days per year in the earlier period. In the later period, the spread has decreased, yet it remains the largest among all clusters. The median value increases slightly for clusters C1, C2 and C4 in the later period and decreases slightly for C3. The largest change can be found in C5, where the median in the later period is lower than the interquartile range in the earlier period. The number of days in C5 decreases from 21.7% to 16.8%.

Composites of VEL, PV and $QG\omega$ for the five jet configurations are shown in Figure 3. We focus only on the forcing generated in the upper troposphere/lower stratosphere, averaging positive and negative values separately to avoid cancellation (as described in section 2.3). The key characteristics of each cluster are briefly summarized in Table 1. Cluster C1 features a double-jet structure to the west and east of the continent, with the jets merging along the south coast of Australia (Fig. 3a). The STJ extends across the entire continent, reaching its maximum along its south coast. Cluster C1 coincides with an alternating pattern of positive and negative $QG\omega$ that is located along the poleward side of the STJ. The strongest upper-level forced ascent (negative $QG\omega$) is located just south of the wind speed maximum along the Australian south coast, sandwiched by two maxima of $QG\omega$ descent. Compared to the overall winter climatology (Fig. 1), the EDJ in C1 is in a similar location to the west of Australia, while the STJ shifts westward. For cluster C2, the jet stream has two wind speed peaks located on either side of the continent (Fig. 3b). To the west, the STJ merges with the EDJ and tilts slightly poleward. In contrast, the STJ to the east is more narrow and zonally oriented. The largest upward motion is located just south of the wind speed maximum and is most clearly visible for the western jet. Over most of the continent, there is a distinct maximum of positive $QG\omega$ and thus forcing of downward motion. Cluster C3 is largely similar to the climatological pattern (Fig. 3c). The STJ is zonally oriented, with its maximum speed over the east coast of Australia. The EDJ is located southwest of Australia and is tilted slightly poleward. The strongest upper-level forced ascent ($QG\omega$ minimum) is discernible just south of the maximum wind speeds and the strongest descent ($QG\omega$ maximum) is located to the west. The $QG\omega$ pattern is zonally elongated and, in particular, does not exhibit an

https://doi.org/10.5194/egusphere-2026-4836
Preprint. Discussion started: 24 August 2026

Table 1. Key characteristics of the jet stream configurations and anomalously wet regions for the five clusters C1-5.

cluster	key characteristics	anom. wet region(s)
C1	strong, partially merged jet with maximum over south coast	west coast & Tasmania
C2	merged jet west of continent and second STJ maximum east of continent	Tasmania
C3	strong STJ with maximum over east coast, most similar to climatology	south coast & Tasmania
C4	weakest STJ and most elongated EDJ, the two jets exhibit comparable wind speeds	east coast
C5	strong STJ with the maximum over the Australian west coast and an absent EDJ	east & west coast

alternating pattern of forced ascent and descent. Instead, the two regions of positive and negative $QG\omega$ overlap. Cluster C4 is characterized by a clear double-jet structure (Fig. 3d). It features the most elongated EDJ and the weakest STJ among all clusters, with comparable wind speeds in the two jets. The EDJ reaches its peak values south of the continent, whereas the STJ exhibits two peaks, one over the Australian west coast and the other to the east of the Australian east coast. A band of positive $QG\omega$ spreads along the STJ, and there are two regions of weak negative $QG\omega$ next to the west coast and over the east coast. Finally, for cluster C5, the STJ is strongest over the Australian west coast and exhibits another maximum in the South Pacific (Fig. 3e). Similarly to cluster C1, there is an alternating pattern of negative and positive $QG\omega$ discernible along the STJ. The strongest upper-level forced ascent ($QG\omega$ minimum) is found just south of the highest wind speeds over the west and south coasts of Australia. A second $QG\omega$ minimum is located at the poleward entrance of the second wind maximum east of the Australian east coast. In all clusters, there are no jets located over New Zealand or the Tasman Sea.

In contrast to Gillett et al. (2021), we find large variability in the wintertime jet stream. Using the clustering approach, we identified five jet configurations, which occur with similar frequency, and which sometimes differ quite considerably in structure from climatology (Fig. 3). However, our results are not contradictory to Gillett et al. (2021), as we use a different method to detect the jet. While Gillett et al. (2021) mainly focus on the intensity and latitude of the strongest winds in the jet stream using zonally averaged, monthly mean zonal winds, we are more interested in the day-to-day variability and the spatial structure of the jet using daily fields of vertically-averaged wind speeds. Hence, although there may be little variability in the intensity and latitudinal position of the jet stream in a zonal and monthly average, the geographical jet structure can differ considerably on shorter time scales. When we examine the day-to-day jet pattern, and summarize the variability into the five clusters, we can clearly demonstrate that the dominant variability of the jet lies in its longitudinal position, including cases of partially displaced or merged jets. Thus, using the zonal mean masks most of the variability in the wintertime subtropical jet and must be interpreted with care. Arakelian and Codron (2012) came to a similar conclusion, namely that the wintertime jet stream often deviates from its mean state. The jet configurations generally correspond to the finding of Lee and Kim (2003), who argues that a weaker STJ is associated with a stronger EDJ, and vice versa.

https://doi.org/10.5194/egusphere-2026-4836
Preprint. Discussion started: 24 August 2026

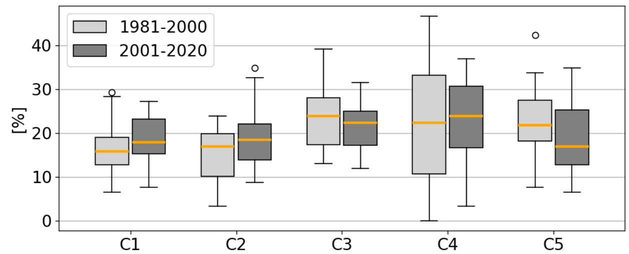

Figure 2. Median and spread of the number of days per year (in percentage) for each cluster are shown for the period from 1981-2000 (light gray) and 2001-2020 (dark gray). The box shows the interquartile range with the upper bound at the 75th percentile, the lower bound at the 25th percentile, and the orange line at the median (i.e., 50th percentile). The upper and lower whiskers correspond to the highest and lowest percentages within 1.5 times the interquartile range. Outliers (i.e., values outside that range) are represented by the circles.

3.2 Characteristics of surface weather

In addition to the differences in upper-level forcing of ascent/descent ($QG\omega$) for the clusters, we now examine the surface weather (mean sea level pressure and precipitation anomalies) associated with each cluster individually (Fig. 4). Note that regions with anomalously high precipitation levels in each cluster are also summarized in Table 1.

Clusters C1 and C5 exhibit the largest positive precipitation anomalies, with C1 producing a maximum along the south coast of Australia and in Tasmania (Fig. 4a), and C5 exhibiting a maximum along the west and south coasts of Australia (Fig. 4e). For C5, an additional maximum is discernible just east of the continent (Fig. 4e), while C2 has a maximum southwest of the continent (Fig. 4b). All of these anomalously wet regions coincide with regions where $QG\omega$ is at its minimum (i.e., strongest upper-level forcing for ascent). Cluster C4 has anomalously wet conditions along the Australian east coast (Fig. 4d). Notably, although the east coast lies in a region of overlapping positive and negative $QG\omega$, the local $QG\omega$ minimum is located over the anomalously wet region, while the maximum $QG\omega$ is shifted to its west. A similar pattern can be found over the Australian east coast in cluster C2 (Fig. 4b), but this is associated with an anomalously dry east coast. In cluster C3, both the west and east coasts of Australia are anomalously dry, with anomalously wet regions in Tasmania and around Melbourne (Fig. 4c).

The strongest precipitation anomalies are found in the tropics for clusters C2 and C5. However, it should be noted that this region also experiences the heaviest precipitation from a climatological perspective, and, therefore, greater anomalies can be expected. The mechanisms of precipitation formation differ substantially in the tropics and extratropics. As our focus is on the influence of the jet stream on precipitation, we will not consider the tropics further. We also calculated precipitation anomalies using AGCD precipitation data, focusing on precipitation over the land. This can be found in the supplementary material (Fig. S3). The distribution of anomalously wet and dry regions in the AGCD data is very similar to that displayed in Fig. 4 based on ERA5, which is, however, more pronounced overland.

https://doi.org/10.5194/egusphere-2026-4836
Preprint. Discussion started: 24 August 2026

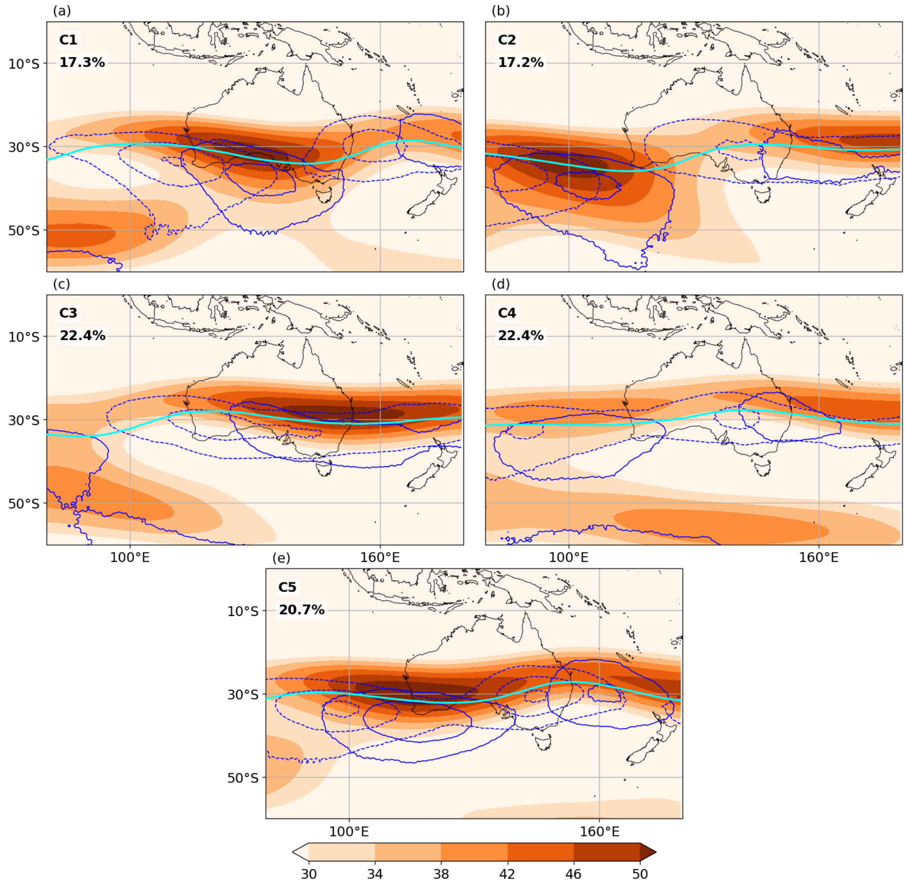

Figure 3. Jet stream configurations (clusters) for winter days. C1-C5 show the mean of all days in the respective cluster, where the shading shows wind speeds (VEL) in m s^{-1} and the contours are the -2 PVU contour at 330 K (cyan) and $QG\omega$ at 500 hPa (blue). The solid $QG\omega$ lines show the forcing of upward motion in Pa s^{-1} (-0.048, -0.032, -0.016) and the dashed lines show the forcing of downward motion (0.016, 0.032, 0.048).

Along with the varying precipitation patterns, the clusters also vary in the pattern of mean sea level pressure. Generally, there is a band of high pressure in the subtropics (subtropical ridge) and lower pressure to the south of it. Cluster C1 exhibits two high-pressure systems, one upstream of the Australian west coast and one over the Australian east coast, respectively. A weak trough is discernible over the Great Australian Bight (Fig. 4a). Clusters C2 and C3 feature a highly elongated high-pressure band stretching from the Indian Ocean to the Australian continent (Fig. 4b and c). Finally, cluster C4 shows a high-pressure system located over most of the continent (Fig. 4d), and for cluster C5 a high-pressure system is discernible in the Indian Ocean, with a surface trough to the southwest of Australia (Fig. 4e).

https://doi.org/10.5194/egusphere-2026-4836
Preprint. Discussion started: 24 August 2026

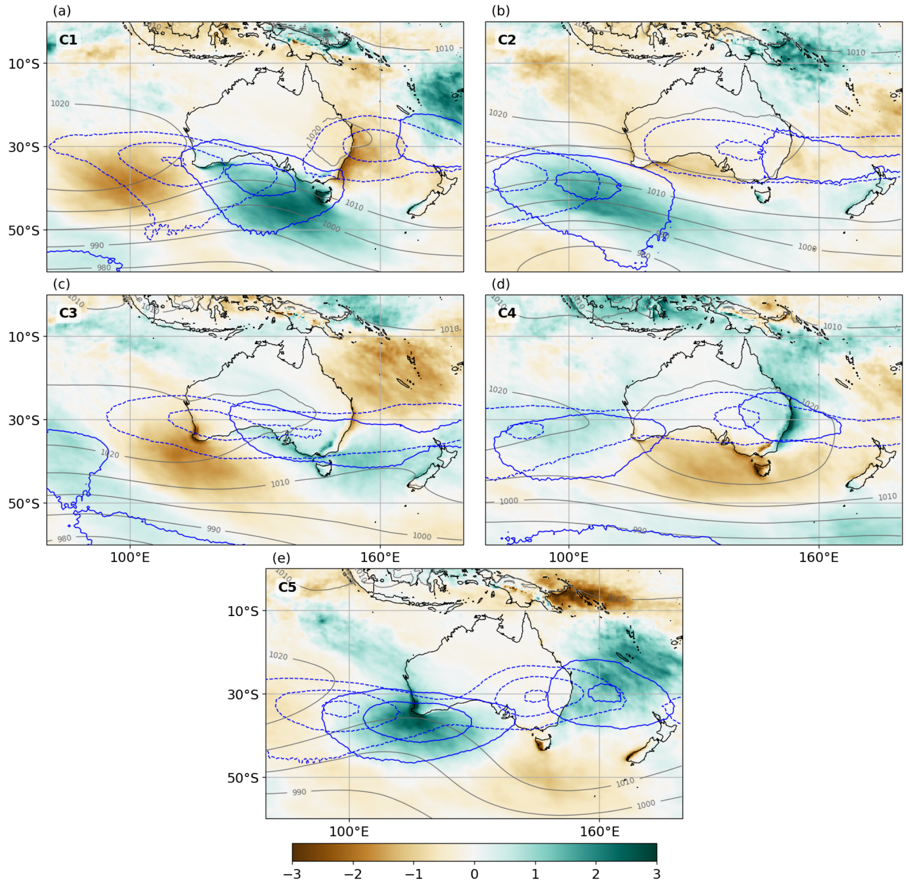

Figure 4. Precipitation anomaly shown for each cluster. The shading illustrates the precipitation anomaly (in mm day^{-1}) compared with the winter climatology using precipitation data from ERA5. The climatology is in the supplementary material (Fig. S2). The blue contours show negative (solid) and positive (dashed) $QG\omega$ at 500 hPa (levels as in Fig. 3) and the grey contours show the mean sea level pressure in hPa.

In summary, analyzing the characteristics of the jet configurations clearly demonstrates the relevance of the jet stream and its variability for precipitation formation (Fig. 4). The regions of enhanced precipitation and upward $QG\omega$ forcing largely coincide. The strongest upper-level forced ascent is located just south of the jet maximum and the vertical motion generally exhibits an alternating pattern of upward and downward motion along the poleward side of the STJ. However, our results do not immediately align with the conceptual 4Q model proposed by Beebe and Bates (1955). This may be due to averaging over many days, which causes important jet characteristics, such as the influence of the orientation or curvature of the jet on the distribution of vertical motion, to be lost (Keyser and Shapiro, 1986; Moore and Vanknowe, 1992; Auestad et al., 2024). We will further discuss these aspects in section 6.

https://doi.org/10.5194/egusphere-2026-4836
Preprint. Discussion started: 24 August 2026

4 Extreme precipitation events

In the previous section, we showed that the different jet configurations are associated with certain regions being anomalously wet, this section examines whether extreme precipitation events occur more frequently in specific clusters. To this end, we have defined extreme precipitation events (EPEs) for six different Australian capital cities (Adelaide, Brisbane, Hobart, Melbourne, Perth, and Sydney) and for three different accumulation periods (daily, 3-day sum, and 5-day sum), as described in Section 2.1. EPEs are defined as events exceeding the 99.5th percentile, and days falling within these events are considered as extreme precipitation days (EPDs). The following sections focus on research questions 3 and 4 raised in the introduction, i.e., how EPEs in the cities are linked to the jet stream configurations, what specific role the jets play in precipitation formation and to which degree days with extreme precipitation differ from the climatology with all days in a cluster included.

Table 2 lists the percentage of EPDs in each cluster for every city. For each city, one or two clusters are much more prominent (with higher percentages of EPDs) than the others. Specifically, in Brisbane and Sydney, the most dominant cluster is C4. However, C5 also accounts for around 30% of EPDs in Sydney. In Hobart, most EPDs occur in C1, whereas in Perth, most events occur in C1 and C5. In Perth, the percentage of EPDs in C1 decreases as the event accumulation period increases, while the percentage in C5 increases (except for 3-day events). In Adelaide, most EPDs occur in C3, while in Melbourne, most events occur in C3 and C5. Finally, Brisbane has the highest percentage of EPDs in a single cluster, with 60-70% of all EPDs occurring in C4.

In the following sections, we focus on EPDs of 5-day events in Perth, Brisbane, Sydney and Hobart, and the cluster in which most of the EPDs occur. By setting the focus on a 5-day accumulation period, we consider extreme precipitation events that are (typically) governed by the large-scale flow situation, in contrast, e.g., to 1-day events, where shorter-scale and more localized processes might be more relevant. However, we will briefly address the sensitivity of the results to the accumulation periods later in Section 4.5. Composites are created separately using all days within a cluster and only EPDs within that cluster (Figs. 5 − 9). The sample sizes for the all-day composite and EPD-only composites differ substantially. Therefore, to ensure that the observed differences are actually associated with the EPDs and not due to the averaging of a larger number of days, we constructed the composite by randomly selecting days within a cluster, while keeping the number of days the same as the number of EPDs in that cluster. These composites created using randomly selected days (not shown) confirm that the observed characteristics are unique to EPDs and are not due to the varying number of days.

The synoptic patterns for Adelaide and Melbourne are not discussed in detail here, but the corresponding composites can be found in the supplementary material (Figs. S17 − S25). In general, the two cities exhibit synoptic patterns that are similar to those of the other cities, particularly Perth. The focus here is on the other four cities, because their associated extreme precipitation events can be more clearly assigned to a specific jet configuration, and they also differ more distinctly from one another.

https://doi.org/10.5194/egusphere-2026-4836
Preprint. Discussion started: 24 August 2026

Table 2. The number of EPDs per cluster is shown as a percentage, rounded to one decimal place, for each city and for three different accumulation periods: daily, 3-day and 5-day sum. The city with the highest percentage of EPDs for each accumulation period is highlighted in bold.

city	acc. period	C1	C2	C3	C4	C5
Adelaide	daily	5.0	25.0	**40.0**	10.0	20.0
	3-day	13.0	19.6	**34.8**	8.7	23.9
	5-day	10.3	8.6	**41.4**	8.6	31.0
Brisbane	daily	10.0	5.0	0.0	**70.0**	15.0
	3-day	0.0	5.6	2.8	**61.1**	30.6
	5-day	2.3	7.0	7.0	**63.8**	20.9
Hobart	daily	**45.0**	25.0	15.0	5.0	10.0
	3-day	**40.5**	11.9	31.0	9.5	7.1
	5-day	**35.4**	12.5	31.3	12.5	8.3
Melbourne	daily	10.0	25.0	25.0	10.0	**30.0**
	3-day	12.5	17.5	**27.5**	15.0	**27.5**
	5-day	11.8	19.6	**27.5**	13.7	**27.5**
Perth	daily	**45.0**	0.0	0.0	15.0	40.0
	3-day	**42.9**	7.1	11.9	14.3	23.8
	5-day	23.7	1.7	16.9	13.6	**44.1**
Sydney	daily	0.0	25.0	0.0	**45.0**	30.0
	3-day	7.9	26.3	0.0	**36.8**	28.9
	5-day	9.3	14.0	9.3	**39.5**	27.9

4.1 Perth

In Perth, 44.1% of the EPDs occur in cluster C5 (Table 2). Figure 5 shows the all-day and EPDs-only composites for C5. The two composites exhibit a very similar location of the STJ (Fig. 5a and b). However, the jet maximum across the west coast to the central continent is stronger and covers a larger area in the EPD-only composite than in the all-day composite (Fig. 5b). The $QG\omega$ dipole is strengthened, with the $QG\omega$ minimum, i.e., maximum upward forcing, located over Perth. The -2 PVU contour, .i.e., the dynamic tropopause, is located along the poleward side of the jet maximum and an amplified PV trough is visible downstream of the strong STJ. While the -2 PVU contour along the strong STJ is similar for all days and EPDs, the downstream development is somewhat stronger for EPDs. This is not reflected in the magnitude of the downstream $QG\omega$ dipole.

https://doi.org/10.5194/egusphere-2026-4836
Preprint. Discussion started: 24 August 2026

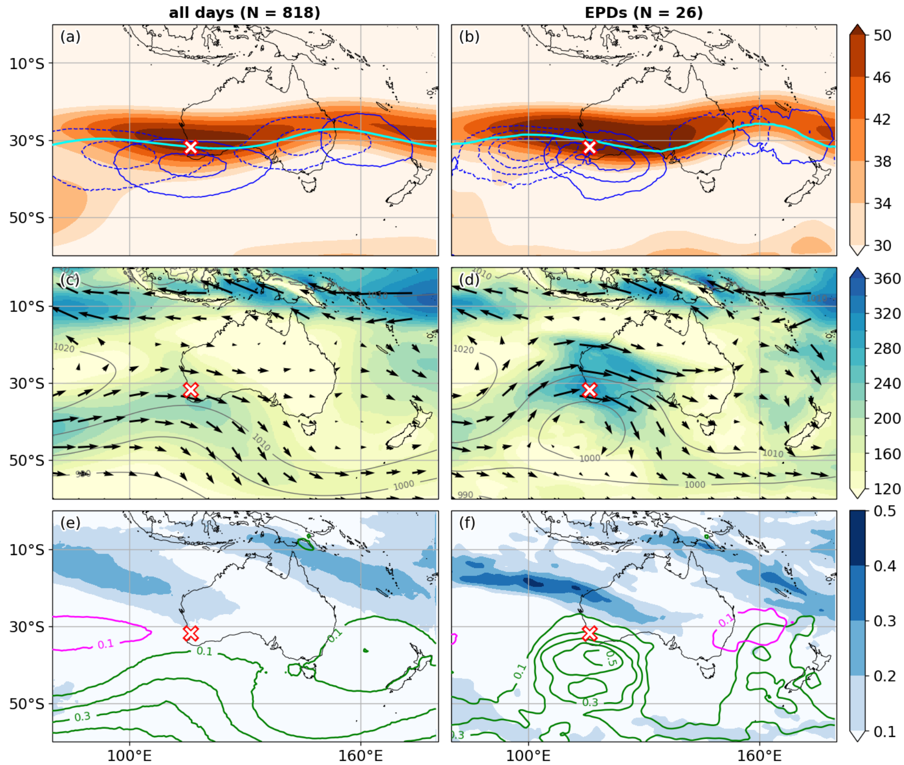

Figure 5. All-day composite (N = 818; a, c, e) and Perth EPD-only composite (N = 26; b, d, f) for cluster C5. (a) and (b) show the wind speed (VEL) in ms^{-1} in the shading, and the contours show the -2 PVU contour at 330 K (cyan) and $QG\omega$ at 500 hPa in Pa s^{-1} (blue) at $\pm$ (0.02, 0.04, 0.06, 0.08) with solid contours for negative values (upward forcing) and dashed contours for positive values (downward forcing). The shading in (c) and (d) shows the magnitude of the IVT (in kg ms^{-1}), the arrows show the IVT as vectors and the grey contours the mean sea level pressure. (e) and (f) show the frequency of fronts in the shading, and the coloured contours the frequencies of cyclones (green) and PV streamers at 330 K (magenta) with intervals of 0.1. The contours of the weather feature frequencies in the EPD-only composite (f) are quite noisy due to the small number of days included in the composite. Therefore, a weak smoothing filter was applied to the three fields (frequency of cyclones, fronts and PV streamers) in the EPDs. The cross marks the location of Perth.

Figures 5c) and d) depict the IVT and mean sea level pressure (MSLP). For EPDs, the IVT is stronger and shifted equatorward (Fig. 5d) compared to the composite for all days. The largest values are found over the west coast of Australia, with a local maximum just over Perth. A surface trough is present in the same region as the enhanced IVT. The frequencies of cyclones, fronts, and PV streamers are shown in Figure 5e) and f). In C5, cyclones can be observed to the south of the jet maximum and fronts to the north of it (Fig. 5e). The frequency of cyclones increases for EPDs (Fig. 5f). Additionally, a higher frequency of fronts is observed in the same region, north of the increased cyclone frequency and on the equatorward side of the jet stream maximum. An increase in the frequencies of cyclones and PV streamers is also evident downstream of the strong STJ.

https://doi.org/10.5194/egusphere-2026-4836
Preprint. Discussion started: 24 August 2026

4.2 Brisbane

Figure 6 shows the same as Figure 5 but for EPDs in Brisbane and cluster C4. 63.8% of all EPDs of 5-day events in Brisbane can be attributed to C4 (Table 2). Comparing Figure 6a) with b), the STJ on the east coast shifts northwards and weakens in the EPD-only composite compared to the all-day composite. Meanwhile, the STJ intensifies further upstream on the Australian west coast. The EDJ is also stronger, and its maximum being slightly shifted to the east in the EPD-only composite. A weak $QG\omega$ minimum lies over the Australian east coast in C4, which is noticeably more pronounced for the EPDs, and, consistently, a PV trough is discernible to the west of Brisbane, located in the centre of a strong $QG\omega$ dipole.

The composites made from all days and EPDs show similar IVT and MSLP patterns in the midlatitudes, with similar pressure gradients and IVT magnitude (Fig. 6c and d). The IVT features a general eastward transport to the south of the continent. For the EPDs, a strong westward IVT lies over the tropics, turning anticyclonically over the Coral Sea and directing poleward along the east coast of Australia towards Brisbane. This is accompanied by a substantially enhanced magnitude over the tropical Pacific and along the east coast (Fig. 6d).

Figure 6e) shows the frequency of the three weather features considered in the Brisbane area, and Figure 6f) the corresponding frequencies for EPDs. They all occur more frequently in the region of interest for EPDs. In particular, the area of enhanced cyclone activity coincides with the region where PV streamers become more frequent, indicating that PV streamers are associated with the development of surface cyclones (Hoskins et al., 1985).

4.3 Sydney

In Sydney, 39.5% of EPDs of 5-day events can be attributed to cluster C4 (Table 2). Unlike in Brisbane, the STJ over the Australian east coast is stronger for EPDs. There is no apparent difference in the -2 PVU contour between the all-day and EPDs-only composites (Fig. 7a and b). The STJ is also stronger upstream of Sydney, and the $QG\omega$ dipole is stronger with the $QG\omega$ minimum located over Sydney.

In the EPDs-only composite, the moisture is transported southward from the tropics along the Australian east coast and then turns eastward (Fig. 7d). Although there is some cyclone and PV streamer activity discernible in the region around Sydney in C4 (Fig. 7e), we observe an increase in cyclone and front frequencies in the region for EPDs (Fig. 7f). This enhanced cyclone frequency is concentrated along the coastal zone, implying that it is related to the development of East Coast Lows, which are known to bring heavy precipitation to the Sydney region (Pepler et al., 2014). In contrast to Brisbane, the frequency of PV streamers does not increase.

The cluster with the second highest number of EPDs of 5-day events in Sydney is C5, accounting for 27.9% (Table 2). In this cluster and for EPDs (Fig. 8b), the STJ is stronger upstream of Sydney and displaced to the north over the Australian east coast compared to its climatological position (Fig. 8a). The -2 PVU contour points to an increased frequency in PV streamers downstream of the strong STJ, and a stronger $QG\omega$ dipole is located over Sydney. Furthermore, the EDJ south of Sydney is stronger.

https://doi.org/10.5194/egusphere-2026-4836
Preprint. Discussion started: 24 August 2026

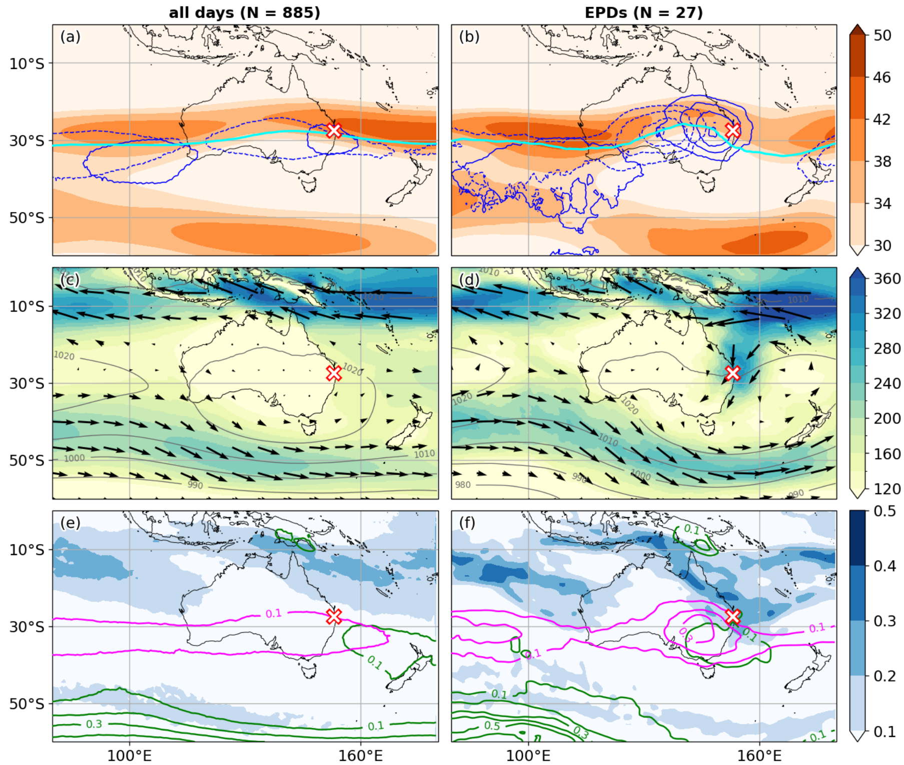

Figure 6. As Fig. 5 but for Brisbane and C4.

Figure 8d) indicates that the moisture is advected towards Sydney from two different directions, with most moist air originating from the tropics. Moisture is transported southward along the Australian east coast, as shown in Figures 6d) and 7d). Additionally, moisture is transported from the tropics of the Indian Ocean across the continent towards the east coast of Australia. Comparing Figure 8e) and f) reveals an overall increase in the frequency of all the weather features considered around Sydney. In addition, cyclone and front frequencies increase in the upstream region over the west coast of Australia, where the jet maximum is located. The regions of enhanced cyclone and PV streamer frequencies overlap, again indicating that surface cyclone formation is supported by upper-level PV evolution.

4.4 Hobart

In Hobart, 35.4% of the EPDs of 5-day events are in cluster C1 (Table 2). This cluster is characterized by the merging of the STJ and EDJ over the south coast of Australia (Fig. 9a). For EPDs, the maximum wind speed of the merged jets is located slightly further southeast, with Hobart situated at the poleward exit of the jet maximum (Fig. 9b). Compared to the all-day composite, the wind speeds are slightly lower, and the jet is a bit broader for EPDs. The -2 PVU contour is similar for the composite of all days and EPDs and lies north of Hobart with a rather zonal orientation. Unlike in Perth, Sydney and Brisbane,

https://doi.org/10.5194/egusphere-2026-4836
Preprint. Discussion started: 24 August 2026

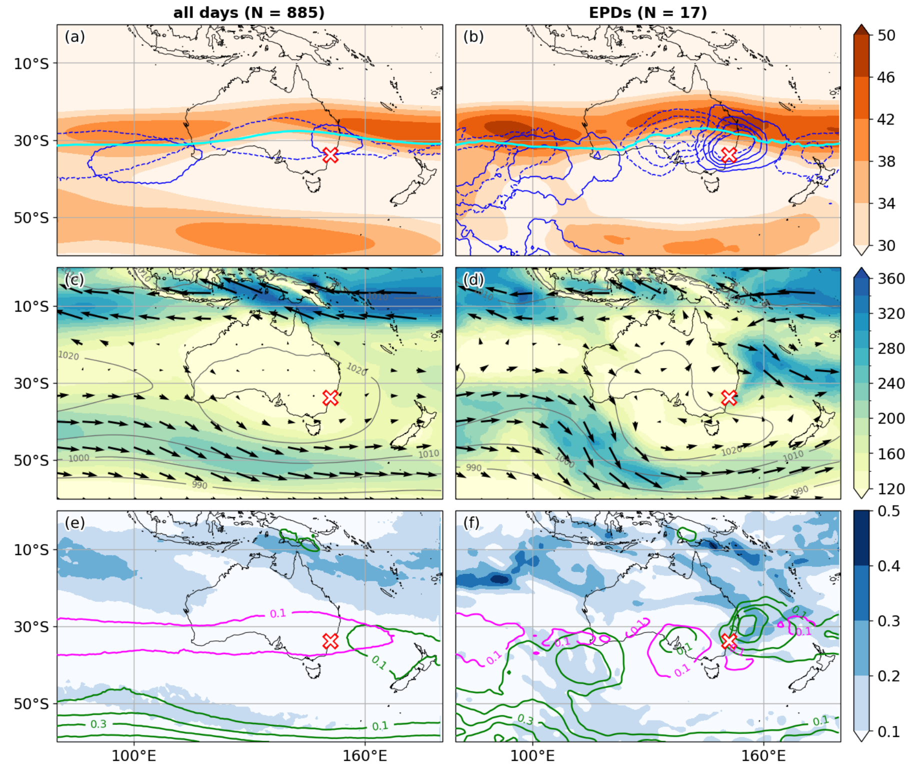

Figure 7. As Fig. 5 but for Sydney and C4.

there is no strengthening of the $QG\omega$ dipole for EPDs, and thus the $QG\omega$ minimum is considerably weaker over Hobart. This indicates that upper-level forcing is less relevant for EPDs in Hobart.

Hobart is located in a region with a strong pressure gradient (Fig. 9d). Unlike the all-day composite (Fig. 9c), the pressure gradient and IVT are notably higher for EPDs (Fig. 9d). In fact, the IVT has its highest values over the Bass Strait, and its vector is oriented perpendicular to the topography of Tasmania, indicating that orographic lifting of the high IVT is important (cf. Fig. 1). Unlike the patterns observed for other capital cities, Hobart's EPDs feature a highly zonal IVT pattern characterized by tropical easterlies and midlatitude westerlies. Of the weather features considered, only an increase in cyclones can be observed in the region around Hobart (Fig. 9f). In contrast to the other cities, there is no clear increase in the frequency of fronts, which likely reflects the fact that vertical lifting due to frontal circulations is much less important than mechanical orographic lifting.

4.5 Sensitivity to accumulation periods

In the previous sections, we focused on 5-day events in different cities. However, similar analyses are also conducted for daily and 3-day events, for the clusters with the highest percentages in each case (as listed in Table 2). All corresponding figures can be found in the supplementary material. In Brisbane and C4, we find that there are only minor differences in the synoptic

https://doi.org/10.5194/egusphere-2026-4836
Preprint. Discussion started: 24 August 2026

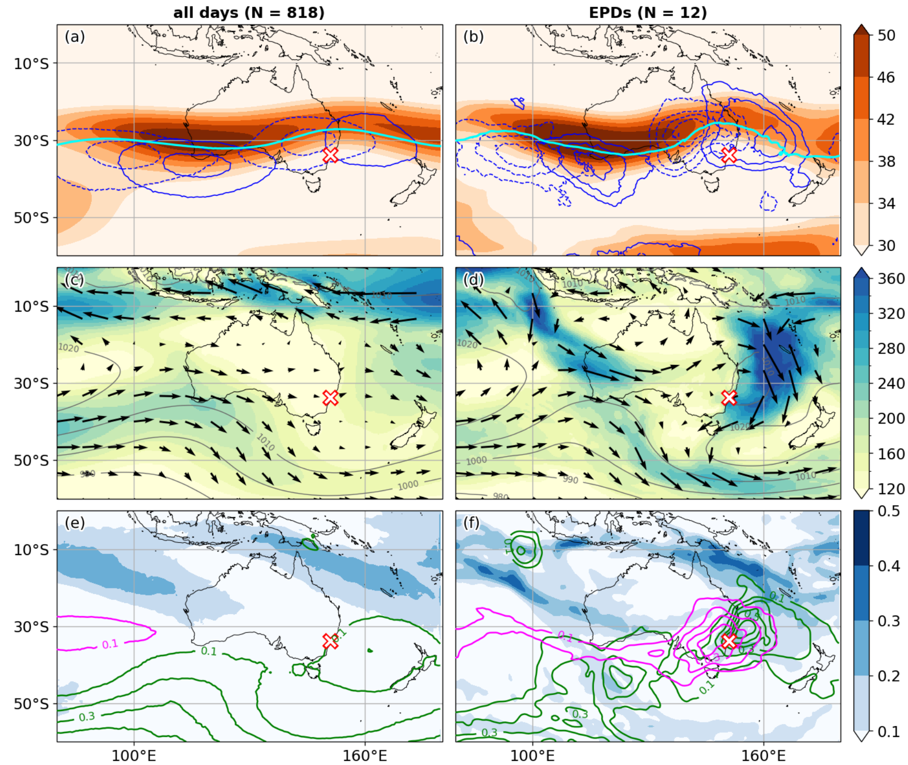

Figure 8. As Fig. 5 but for Sydney and C5.

patterns regardless of the accumulation period (Fig. 6, Fig. S4 and Fig. S5). The change in weather feature frequencies between the all-day and EPDs-only composites is also very similar. The same applies for Hobart and C1 (Fig. 9, Fig. S10 and Fig. S11), and Sydney and C5 (Fig. 8, Fig. S8 and Fig. S9). The characteristics of the 5-day events are also discernible for the daily and 3-day events. If we look at Sydney and C4, we can see that the intensification of the jet stream observed for 5-day events (Fig. 7) is less pronounced for daily and 3-day events (Fig. S6 and S7). Unlike for 5-day events, the frequency of PV streamers is increased in the region around Sydney for daily and 3-day events. For Perth, we observe a shift of EPDs from C1 to C5 as the accumulation period increases. Therefore, for shorter extreme precipitation events, the highest percentage is not found in cluster C5, but in C1. Both clusters are characterized by an intensification of the jet stream. However, unlike C5 (Fig. 5, Fig. S12 and Fig. S13), C1 exhibits a more poleward-oriented jet stream. Perth is located in the poleward entrance region of the jet stream, and there is an additional increase in the frequency of PV streamers (Fig. S14-S16). The jet stream is strongest is C1 for daily and 3-day events, whereas it is strongest in C5 for 5-day events. These are the clusters with the highest percentage of EPDs, respectively.

https://doi.org/10.5194/egusphere-2026-4836
Preprint. Discussion started: 24 August 2026

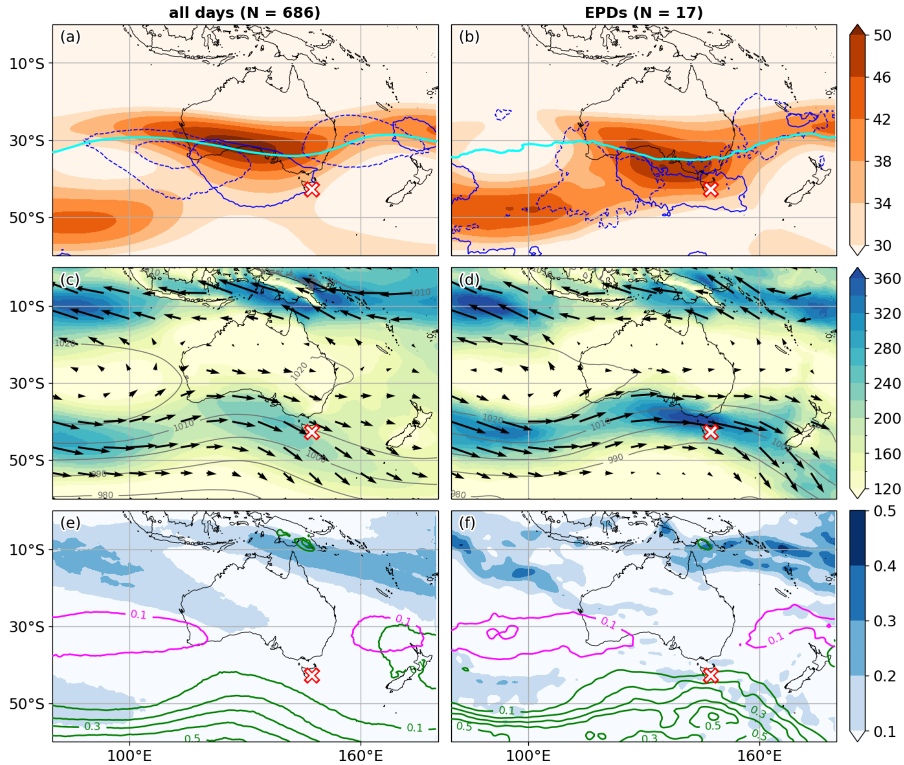

Figure 9. As Fig. 5 but for Hobart and C1.

5 Discussion

In every city, a higher percentage of EPDs is found in one or two clusters (Table 2). This suggests that jet streams play an important role in triggering or maintaining extreme precipitation events. The cluster with the highest number of EPDs remains consistent regardless of the duration (accumulation period) of the events. Perth is the exception, with a decreasing percentage of EPDs for C1 and an increasing percentage for C5 with longer durations. Brisbane has the highest number of EPDs associated with a cluster, accounting for 60-70% of all EPDs (Table 2), suggesting that the jet stream is relevant not only for extratropical precipitation, but also for subtropical precipitation.

We found that extreme precipitation events are associated with two main jet patterns. The first pattern (Fig. 10a) is characterized by a strengthened STJ north of the precipitating area, together with an undisturbed -2 PVU contour along the jet. In this configuration, the jet stream acts as a waveguide for surface weather systems, e.g., cyclones and associated fronts, that propagate downstream along it. In accordance with this, PV streamers develop downstream of the strong jet, where hence the waveguide becomes more perturbed. We also observe an increase in the frequency of cyclones and fronts in the region of interest. Furthermore, the $QG\omega$ dipole is amplified and the $QG\omega$ minimum is located over the region of extreme precipitation.

https://doi.org/10.5194/egusphere-2026-4836
Preprint. Discussion started: 24 August 2026

This points to the importance of large-scale dynamic lifting. This is the main pattern for EPDs in Perth, where we found that the EPDs in C5 are associated with a stronger STJ (Fig. 5). Our results also support those of Frederiksen and Frederiksen (2007), who noted that a weaker STJ is associated with decreased precipitation on the west coast of Australia. Additionally, we found that Sydney EPDs in C4 are associated with a stronger STJ, a stronger $QG\omega$ dipole, an undisturbed -2 PVU contour, and an increase in the cyclone and front frequency (Fig. 7). Consistent with our findings, Lehmann and Coumou (2015) noted an increase in extreme precipitation events associated with anomalously zonal and/or fast jet streams. This further emphasizes that weather can be affected not only by particularly wavy jet streams, but also by relatively straight and zonal ones, whereby stronger jet streams have been found to be correlated with decreased variability in latitude (Woollings et al., 2018). Similarly to the described pattern (Fig. 10a), Risbey et al. (2009) found that the STJ is intensified in regions of enhanced precipitation. However, while they found precipitation mainly in the poleward exit region of the jet, we found precipitation south of the jet maximum, where it coincided with the area of stronger upper-level forced ascent.

The second pattern (Fig. 10b) shows a weaker STJ in the region of interest. This STJ is displaced slightly north of its climatological position. An enhanced PV streamer frequency and an amplified $QG\omega$ dipole are discernible in this region, which is also characterized by a higher frequency of cyclones and fronts. A stronger STJ occurs upstream of the PV streamer location. Most EPDs in Brisbane are associated with this pattern, and additionally, EPDs in Sydney in C5 (Figs. 6 and 8). In C5, Sydney is located downstream of the strong STJ, where the STJ is weaker and the PV streamer frequency is higher. These two examples are consistent with the findings of Maher and Sherwood (2016), who found that a weaker STJ generally leads to increased precipitation on the east coast of Australia. These results are also consistent with those of Gu et al. (2025), who found enhanced precipitation in regions of reduced wind speeds between two jet cores. They showed that these regions are associated with tropopause folding, which induces ascent and leads to increased precipitation. We observe a higher frequency of PV streamers in connection with a weaker STJ, and a similar mechanism is conceivable. Unlike in Figure 10a), the enhanced PV streamer frequency is co-located with the extreme precipitation events here.

Extreme precipitation events at a specific location do not have to be associated with just one of the two patterns, but they can be caused by either of them (as for Sydney). For example, cluster C5 demonstrates that these two patterns can also occur with the same jet configuration, with a stronger STJ upstream and an increased PV streamer frequency downstream in the region where the STJ weakens. Comparison of Figures 5b) and 9b) highlights that the jet pattern is similar for both cities, except that extreme precipitation occurs in Perth in the region of the strong STJ and in Sydney where the STJ is weakened.

In Hobart, we observe a third potential influence of the jet stream on extreme precipitation, whereby the STJ and EDJ merge and a strong IVT is directed perpendicular to the western topography of Tasmania (Fig. 9). As there is no apparent increase in upper-level forcing ($QG\omega$), we assume that the precipitation is rather caused by vertical lifting due to the topography. From a climatological perspective, the western side of Tasmania receives more winter precipitation than the eastern side (Bureau of Meteorology, 2024). The increased IVT may be linked to the merging of the jet streams, with the merged jet stream coinciding

https://doi.org/10.5194/egusphere-2026-4836
Preprint. Discussion started: 24 August 2026

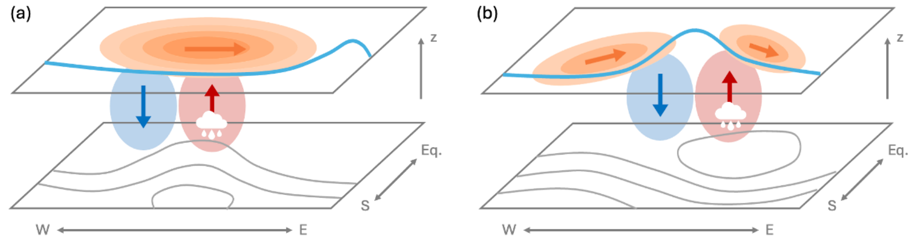

Figure 10. Schematic of jet stream patterns driving extreme precipitation events associated with an intensified (a) and a weaker STJ (b). The jet stream is displayed in orange, with wind speed indicated by the number of orange shadings and arrow length. $QG\omega$ is shown as a vertical arrow in blue for descent and red for ascent. Grey contours indicate mean sea level pressure and the -2 PVU contour, i.e., the dynamic tropopause on an isentropic surface, is shown in blue. The white cloud shows the approximate location of the extreme precipitation relative to the jet stream.

with a strong pressure gradient at the surface. The IVT is directed along the pressure gradient, bringing moisture into the region and causing extreme precipitation. This aligns with Suresan et al. (2025) who found that wind extremes occur during merged jet events, aligning with the jet orientation. These events also significantly impact regional precipitation distribution. Similarly, the merging of the jets could lead to stronger zonal winds extending further into the lower troposphere, oriented perpendicular towards the topography of Tasmania. Further analysis of moisture airstreams is required to determine whether the increased moisture transport is related to large-scale circulation and the merging of the jet streams.

Generally, we find that EPDs are associated with an increase in upper-level forced vertical motion and a stronger moisture flow into the region of interest. As in Zhao et al. (2022), extreme precipitation occurs where there are large values of upper-level forced vertical motion (except in the case of Hobart), and this can happen when the STJ is stronger or weaker. The IVT depends more on the region considered than on the jet configuration. For extreme precipitation on the Australian east coast, the majority of moisture is transported southwards from the tropics along the east coast towards Brisbane and Sydney. For the Australian west coast and Tasmania, moisture is transported from the west into these two regions embedded within the westerly flow. Overall, we find that the IVT for EPDs increases for all cities and generally deviates more strongly from its mean position.

6 Conclusions

We analyzed the variability of the wintertime jet stream over Australia using a K-means clustering approach on vertically-averaged wind speed fields from the ERA5 reanalysis dataset for the winter months from 1980 to 2022. This defined five different jet stream configurations. We then analyzed the distribution of upper-level forced vertical motion and precipitation for these configurations. Furthermore, our analysis of extreme precipitation events in various Australian capital cities (Adelaide, Brisbane, Hobart, Melbourne, Perth, Sydney) reveals the important role that the jet stream plays in driving these events, whereby extreme precipitation events are defined using the Australian Gridded Climate Data (AGCD) to identify events as

https://doi.org/10.5194/egusphere-2026-4836
Preprint. Discussion started: 24 August 2026

those exceeding the 99.5th percentile, primarily focusing on a 5-day accumulation period. Based on our analysis, the four research questions raised in section 1 can be answered as follows:

1. Generally, the subtropical jet stream has a similar intensity across all clusters (except for C4), but distinct spatial patterns emerge. C1 and C2 exhibit a partially merged jet stream, with C1 showing the jet maximum over the Australian south coast and C2 showing maxima to the west and east of the continent. C3 shows a strong STJ with the jet maximum located over the Australian east coast. This pattern most closely resembles the winter climatology. C4 exhibits the weakest STJ and the most elongated EDJ, with comparable wind speeds in both jet streams. Finally, C5 exhibits a strong STJ with the maximum located on the west coast of Australia. We find that the variability of the winter jet stream is particularly discernible in the longitudinal position of the jet maximum, whereas its latitudinal position is much less affected.

2. In the mean, the upper-level forced vertical motion is generally characterized by an alternating pattern of upward and downward motion along the poleward side of the STJ. The strongest upward motion occurs just south of the jet maximum. The different jet configurations are associated with different anomalously wet or dry regions, demonstrating the relevance of the jet stream for precipitation. The largest anomalies are found in the coastal areas of the extratropics where the regions of enhanced precipitation and upward motion largely coincide.

3. The majority of extreme precipitation events in all of the studied cities are associated with one or two jet configurations, implying that the jet stream plays an important role in triggering or maintaining these events. There are two main jet stream patterns associated with extreme precipitation. The first pattern features a stronger STJ in the precipitating area, acting as a waveguide for surface weather systems that propagate along it. The synoptic patterns of the corresponding clusters show an increase in cyclone and front frequencies near the jet maximum, while the -2 PVU contour remains relatively undisturbed. The second pattern features a weaker STJ that enables the formation of PV streamers and results in extreme precipitation combined with an increase in cyclone and front frequencies. The STJ is weaker and displaced northwards, with a PV trough observed in the region of the weak STJ. Both patterns are accompanied by an amplification of the $QG\omega$ dipole, emphasizing the importance of upper-level forced upward motion for extreme precipitation events. Specifically, the $QG\omega$ minimum, i.e., strongest upward motion, coincides with the location of the extreme precipitation.

4. The pattern featuring a strong STJ in the precipitation area is primarily responsible for 5-day extreme precipitation events in Perth, while the pattern featuring a weakened STJ is the main driver of such events in Brisbane. In Sydney, we found that 5-day extreme precipitation events are associated with both patterns, during which the STJ was weakened or strengthened. In Hobart, a third possible influence of the jet stream on precipitation can be observed. The merging of the EDJ and STJ likely leads to strong zonal, low-tropospheric winds associated with increased moisture transport that impinges on Tasmania's western topography. This moist airstream is then orographically forced to ascend, causing extreme precipitation events there. Along the Australian east coast (Brisbane and Sydney), most of the moisture is transported southwards from the tropics towards the respective cities. Conversely, on the west coast, moisture is brought

https://doi.org/10.5194/egusphere-2026-4836
Preprint. Discussion started: 24 August 2026

toward Perth via an equatorward shift of the mean westerly flow, whereas for Hobart, the moisture transport occurs zonally within the mean westerly flow.

The strength of our analysis lies in the description of the spatial distribution of the jet stream configurations, enabling us to describe the characteristics associated with different jet configurations, e.g., $QG\omega$ and surface weather patterns. One of the main limitations of our method for capturing the variability of the wintertime jet stream is the choice of the number of clusters. This leads to averaging over a large number of days, which still masks much of the day-to-day variability. This can result in important properties of the jet stream being lost, such as the effects of the jet orientation or curvature. It would be interesting to characterize the jet in this way and then quantify its effect on the jet-precipitation relationship. Using a larger number of clusters could allow us to capture daily variations more effectively and take into account the effects of more anomalous jet configurations. Finally, the $QG\omega$ pattern does not align with theoretical expectations (Beebe and Bates, 1955), as it is strongly influenced by the curvature and orientation of the jet streaks. Therefore, an object-based approach to jet streak tracking is required to isolate and account for these specific geometric influences on the forced vertical motion (Kuhn et al., 2026). The exact driver of the $QG\omega$ forcing requires some further investigation, particularly with regard to the interactions between PV features, jet streaks, and vertical motion, as discussed in Bukenberger et al. (2023).

In summary, this study has shown that jet streams are essential to better understand and ultimately predict extreme precipitation in Australia. They govern the spatial organization and lifecycle of weather systems and the associated vertical lifting necessary for extreme precipitation events.

Code availability. The code used in this study can be provided by the authors upon request.

Data availability. ERA5 reanalysis is hosted by the National Computational Infrastructure (NCI) at https://dx.doi.org/10.25914/5f48874388857. QGω and weather object datasets can be obtained from Michael Sprenger on request.

Author contributions. Anna Kuhn led this study and was responsible for formal analysis, writing of the original draft, and visualisation. Chenhui Jin and Michael Sprenger contributed to methodology, and all the authors contributed to reviewing, editing and writing.

Competing interests. The authors declare that they have no conflict of interest.

Acknowledgements. The project was undertaken with resources and assistances from the National Computational Infrastructure (NCI), and NCRIS enabled capability supported by the Australian Government. Chenhui Jin and Elizabeth Ritchie are supported by the ARC Centre of Excellence for the Weather of the 21st Century (CE230100012). Special thanks go to Heini Wernli at ETH Zurich for giving us the opportunity to work on this paper.

https://doi.org/10.5194/egusphere-2026-4836
Preprint. Discussion started: 24 August 2026

References

Arakelian, A. and Codron, F.: Southern hemisphere jet variability in the IPSL GCM at varying resolutions, Journal of the Atmospheric Sciences, 69, 3788–3799, https://doi.org/10.1175/JAS-D-12-0119.1, 2012.

Ashcroft, L. C., Pezza, A. B., and Simmonds, I.: Cold events over southern Australia: Synoptic climatology and hemispheric structure, Journal of Climate, 22, 6679–6698, https://doi.org/10.1175/2009JCLI2997.1, 2009.

Auestad, H., Spensberger, C., Marcheggiani, A., Ceppi, P., Spengler, T., and Woollings, T.: Spatio-temporal averaging of jets obscures the reinforcement of baroclinicity by latent heating, Weather and Climate Dynamics, 5, 1269–1286, https://doi.org/10.5194/wcd-5-1269-2024, 2024.

Banderier, H., Tuel, A., Woollings, T., and Martius, O.: Seasonal to decadal variability and persistence properties of the Euro-Atlantic jet streams characterized by complementary approaches, Weather and Climate Dynamics, 6, 715–739, https://doi.org/10.5194/wcd-6-715-2025, 2025.

Beebe, R. G. and Bates, F. C.: A Mechanism for assisting in the release of convective instability, Monthly Weather Review, 83, 1–10, https://doi.org/https://doi.org/10.1175/1520-0493(1955)083<0001:AMFAIT>2.0.CO;2, 1955.

Bell, B., Hersbach, H., Simmons, A., Berrisford, P., Dahlgren, P., Horányi, A., Muñoz-Sabater, J., Nicolas, J., Radu, R., Schepers, D., Soci, C., Villaume, S., Bidlot, J. R., Haimberger, L., Woollen, J., Buontempo, C., and Thépaut, J. N.: The ERA5 global reanalysis: Preliminary extension to 1950, Quarterly Journal of the Royal Meteorological Society, 147, 4186–4227, https://doi.org/10.1002/qj.4174, 2021.

Besson, P., Fischer, L. J., Schemm, S., and Sprenger, M.: A global analysis of the dry-dynamic forcing during cyclone growth and propagation, Weather and Climate Dynamics, 2, 991–1009, https://doi.org/10.5194/wcd-2-991-2021, 2021.

Bösiger, L., Sprenger, M., Boettcher, M., Joos, H., and Günther, T.: Integration-based extraction and visualization of jet stream cores, Geoscientific Model Development, 15, 1079–1096, https://doi.org/10.5194/gmd-15-1079-2022, 2022.

Bukenberger, M., Rüdisühli, S., and Schemm, S.: Jet stream dynamics from a potential vorticity gradient perspective: The method and its application to a kilometre-scale simulation, Quarterly Journal of the Royal Meteorological Society, 149, 2409–2432, https://doi.org/10.1002/qj.4513, 2023.

Bukenberger, M., Fasnacht, L., Rüdisühli, S., and Schemm, S.: A climatological characterization of North Atlantic winter jet streaks and their extremes, Weather and Climate Dynamics, 6, 279–316, https://doi.org/10.5194/wcd-6-279-2025, 2025.

Bureau of Meteorology: Mean monthly, seasonal and annual rainfall data (base climatological data sets), https://www.bom.gov.au/climate/maps/averages/rainfall/?period=dry&region=aus, 2024.

Clark, A. J., Schaffer, C. J., Gallus, W. A., and Johnson-O'mara, K.: Climatology of storm reports relative to upper-level jet streaks, Weather and Forecasting, 24, 1032–1051, https://doi.org/10.1175/2009WAF2222216.1, 2009.

Davidson, N. E., Tory, K. J., Reeder, M. J., and Drosdowsky, W. L.: Extratropical-tropical interaction during onset of the Australian monsoon: Reanalysis diagnostics and idealized dry simulations, Journal of the Atmospheric Sciences, 64, 3475–3498, https://doi.org/10.1175/JAS4034.1, 2007.

Davies, D. L. and Bouldin, D. W.: A Cluster Separation Measure, IEEE Transactions on Pattern Analysis and Machine Intelligence, PAMI-1, 224–227, 1979.

Davies, H. C.: The Quasigeostrophic omega equation: Reappraisal, refinements, and relevance, Monthly Weather Review, 143, 3–25, https://doi.org/10.1175/MWR-D-14-00098.1, 2015.

https://doi.org/10.5194/egusphere-2026-4836
Preprint. Discussion started: 24 August 2026

Davies, H. C., Sprenger, M. A., and Wernli, H.: Quasi-Geostrophic Theory, Encyclopedia of Atmospheric Sciences, pp. 63–76, https://doi.org/10.1016/B978-0-323-96026-7.00085-0, 2026.

Frederiksen, J. S. and Frederiksen, C. S.: Interdecadal changes in southern hemisphere winter storm track modes, Tellus, Series A: Dynamic Meteorology and Oceanography, 59, 599–617, https://doi.org/10.1111/j.1600-0870.2007.00264.x, 2007.

Galfi, V. M. and Messori, G.: Persistent anomalies of the North Atlantic jet stream and associated surface extremes over Europe, Environmental Research Letters, 18, https://doi.org/10.1088/1748-9326/acaedf, 2023.

Gibson, J. K., Kållberg, P., Uppala, S., Hernandez, A., Nomura, A., and Serrano, E.: ERA Description, ECMWF Re-Analysis Project Report Series 1, Tech. rep., ECMWF, Reading UK, 1997.

Gillett, Z. E., Hendon, H. H., Arblaster, J. M., and Lim, E.-P.: Tropical and Extratropical Influences on the Variability of the Southern Hemisphere Wintertime Subtropical Jet, Journal of Climate, 34, 4009–4022, https://doi.org/10.1175/JCLI-D-20, 2021.

Gu, M., Luo, J., Jiang, N., Wang, L., Wang, Z., Luo, F., Zhang, C., Xia, X., and Zhang, J.: Effects of Jet Break on Summer Precipitation in Central Asia, Geophysical Research Letters, 52, https://doi.org/10.1029/2025GL116349, 2025.

Hartigan, J. A. and Wong, M. A.: Algorithm AS 136: A K-Means Clustering Algorithm, Source: Journal of the Royal Statistical Society Series C, 28, 100–108, 1979.

Hauser, S., Grams, C. M., Reeder, M. J., McGregor, S., Fink, A. H., and Quinting, J. F.: A weather system perspective on winter–spring rainfall variability in southeastern Australia during El Niño, Quarterly Journal of the Royal Meteorological Society, 146, 2614–2633, https://doi.org/10.1002/qj.3808, 2020.

Held, I. M. and Hou, A. Y.: Nonlinear Axially Symmetric Circulations in a Nearly Inviscid Atmosphere, Journal of the Atmospheric Sciences, 37, 515–533, 1980.

Hersbach, H., Bell, B., Berrisford, P., Hirahara, S., Horányi, A., Muñoz-Sabater, J., Nicolas, J., Peubey, C., Radu, R., Schepers, D., Simmons, A., Soci, C., Abdalla, S., Abellan, X., Balsamo, G., Bechtold, P., Biavati, G., Bidlot, J., Bonavita, M., De Chiara, G., Dahlgren, P., Dee, D., Diamantakis, M., Dragani, R., Flemming, J., Forbes, R., Fuentes, M., Geer, A., Haimberger, L., Healy, S., Hogan, R. J., Hólm, E., Janisková, M., Keeley, S., Laloyaux, P., Lopez, P., Lupu, C., Radnoti, G., de Rosnay, P., Rozum, I., Vamborg, F., Villaume, S., and Thépaut, J. N.: The ERA5 global reanalysis, Quarterly Journal of the Royal Meteorological Society, 146, 1999–2049, https://doi.org/10.1002/qj.3803, 2020.

Hoskins, B. J. and James, I. N.: The omega equation, in: Fluid Dynamics of the Midlatitude Atmosphere, pp. 225–243, Wiley, https://doi.org/10.1002/9781118526002.ch13, 2014.

Hoskins, B. J., James, I. N., and White, G. H.: The Shape, Propagation and Mean-Flow Interaction of Large-Scale Weather Systems, Journal of the Atmospheric Sciences, 40, 1595–1612, 1983.

Hoskins, B. J., McIntyre, M. E., and Robertson, A. W.: On the use and significance of isentropic potential vorticity maps, Quarterly Journal of the Royal Meteorological Society, 111, 877–946, https://doi.org/10.1002/qj.49711147002, 1985.

Jenkner, J., Sprenger, M., Schwenk, I., Schwierz, C., Dierer, S., and Leuenberger, D.: Detection and climatology of fronts in a high-resolution model reanalysis over the Alps, Meteorological Applications, 17, 1–18, https://doi.org/10.1002/met.142, 2010.

Jin, C., Reeder, M. J., Gallant, A. J., Parker, T., and Sprenger, M.: Changes in Weather Systems during Anomalously Wet and Dry Years in Southeastern Australia, Journal of Climate, 37, 1131–1153, https://doi.org/10.1175/JCLI-D-23-0305.1, 2024.

Jin, C., Gallant, A. J., Parker, T., and Reeder, M. J.: Weather systems and their contribution to seasonal rainfall in Australia, Quarterly Journal of the Royal Meteorological Society, 151, https://doi.org/10.1002/qj.5013, 2025.

Jones, D. A., Wang, W., and Fawcett, R.: High-quality spatial climate data-sets for Australia, Australian Meteorological and Oceanographic Journal, 58, 233–248, https://doi.org/10.22499/2.5804.003, 2009.

Keyser, D. and Shapiro, M. A.: A Review of the Structure and Dynamics of Upper-Level Frontal Zones, Monthly Weather Review, 114, 452–499, https://doi.org/https://doi.org/10.1175/1520-0493(1986)114<0452:AROTSA>2.0.CO;2, 1986.

Koch, P., Wernli, H., and Davies, H. C.: An event-based jet-stream climatology and typology, International Journal of Climatology, 26, 283–301, https://doi.org/10.1002/joc.1255, 2006.

Krishnamurti, T.: The Subtropical Jet Stream of Winter, Journal of the Atmospheric Sciences, 18, 172–191, 1961.

Kuhn, A., Jin, C., Ritchie, E., and Sprenger, M. A.: Variability of the Wintertime Jet Stream over Australia and its Role in Extreme Precipitation Events, https://doi.org/10.3929/ethz-c-000801175, 2026.

Lee, S. and Kim, H.-K.: The Dynamical Relationship between Subtropical and Eddy-Driven Jets, Journal of Atmospheric Sciences, 60, 1490–1503, 2003.

Lehmann, J. and Coumou, D.: The influence of mid-latitude storm tracks on hot, cold, dry and wet extremes, Scientific Reports, 5, 17 481, https://doi.org/10.1038/srep17491, 2015.

Li, C. and Wettstein, J. J.: Thermally driven and eddy-driven jet variability in reanalysis, Journal of Climate, 25, 1587–1596, https://doi.org/10.1175/JCLI-D-11-00145.1, 2012.

Li, X., Zheng, J., Wang, C., Lin, X., and Yao, Z.: Unraveling the roles of jet streams on the unprecedented hot July in Western Europe in 2022, npj Climate and Atmospheric Science, 7, 323, https://doi.org/10.1038/s41612-024-00880-2, 2024.

Limpasuvan, V. and Hartmann, D. L.: Eddies and the annular modes of climate variability, Geophysical Research Letters, 26, 3133–3136, https://doi.org/10.1029/1999GL010478, 1999.

Lorenz, E. N.: Available Potential Energy and the Maintenance of the General Circulation, Tellus A: Dynamic Meteorology and Oceanography, 7, 157–167, https://doi.org/10.3402/tellusa.v7i2.8796, 1955.

Maher, P. and Sherwood, S. C.: Skill in Simulating Australian Precipitation at the Tropical Edge, Journal of Climate, 29, 1477–1496, https://doi.org/10.1175/JCLI-D-15-0548.s1, 2016.

Martin, J. E.: Recent Trends in the Waviness of the Northern Hemisphere Wintertime Polar and Subtropical Jets, Journal of Geophysical Research: Atmospheres, 126, https://doi.org/10.1029/2020JD033668, 2021.

McKay, R. C., Boschat, G., Rudeva, I., Pepler, A., Purich, A., Dowdy, A., Hope, P., Gillett, Z. E., and Rauniyar, S.: Can southern Australian rainfall decline be explained? A review of possible drivers, Wiley Interdisciplinary Reviews: Climate Change, 14, https://doi.org/10.1002/wcc.820, 2023.

Moore, J. T. and Vanknowe, G. E.: The Effect of Jet-Streak Curvature on Kinematic Fields, Monthly Weather Review, 120, 2429–2441, https://doi.org/10.1175/1520-0493(1992)120<2429:TEOJSC>2.0.CO;2, 1992.

Palmén, E.: On the distribution of Temperature and Wind in the upper Westerlies, Journal of the Atmospheric Sciences, 5, 20–27, https://doi.org/https://doi.org/10.1175/1520-0469(1948)005<0020:OTDOTA>2.0.CO;2, 1948.

Pepler, A., Coutts-Smith, A., and Timbal, B.: The role of East Coast Lows on rainfall patterns and inter-annual variability across the East Coast of Australia, International Journal of Climatology, 34, 1011–1021, https://doi.org/10.1002/joc.3741, 2014.

Reinert, P.: Bericht zum Programm zur Berechnung der diagnostischen, quasigeostrophischen Vertikalgeschwindigkeit, Tech. rep., ETH Zurich, https://doi.org/10.3929/ethz-b-000500755, 2009.

Risbey, J. S., Pook, M. J., Mcintosh, P. C., Ummenhofer, C. C., and Meyers, G.: Characteristics and variability of synoptic features associated with cool season rainfall in southeastern Australia, International Journal of Climatology, 29, 1595–1613, https://doi.org/10.1002/joc.1775, 2009.

Rose, S. F., Hobbs, P. V., Locatelli, J. D., and Stoelinga, M. T.: A 10-Yr Climatology Relating the Locations of Reported Tornadoes to the Quadrants of Upper-Level Jet Streaks, Weather and Forecasting, 19, 301–309, 2004.

Schemm, S., Rudeva, I., and Simmonds, I.: Extratropical fronts in the lower troposphere-global perspectives obtained from two automated methods, Quarterly Journal of the Royal Meteorological Society, 141, 1686–1698, https://doi.org/10.1002/qj.2471, 2015.

Seager, R., Kushnir, Y., Nakamura, J., Ting, M., and Naik, N.: Northern Hemisphere winter snow anomalies: ENSO, NAO and the winter of 2009/10, Geophysical Research Letter, 37, https://doi.org/doi:10.1029/2010GL043830, 2010.

Spensberger, C. and Spengler, T.: Feature-based jet variability in the upper troposphere, Journal of Climate, 33, 6849–6871, https://doi.org/10.1175/JCLI-D-19-0715.1, 2020.

Spensberger, C., Reeder, M. J., Spengler, T., and Patterson, M.: The connection between the southern annular mode and a feature-based perspective on southern hemisphere midlatitude winter variability, Journal of Climate, 33, 115–129, https://doi.org/10.1175/JCLI-D-19-0224.1, 2020.

Sprenger, M., Fragkoulidis, G., Binder, H., Croci-Maspoli, M., Graf, P., Grams, C. M., Knippertz, P., Madonna, E., Schemm, S., Škerlak, B., and Wernli, H.: Global climatologies of Eulerian and Lagrangian flow features based on ERA-Interim, Bulletin of the American Meteorological Society, 98, 1739–1748, https://doi.org/10.1175/BAMS-D-15-00299.1, 2017.

Suresan, S., Harnik, N., and Caballero, R.: Extreme weather anomalies and surface signatures associated with merged Atlantic–African jets during northern winter, Weather and Climate Dynamics, 6, 789–806, https://doi.org/10.5194/wcd-6-789-2025, 2025.

Trenberth, K. E.: Storm tracks in the Southern Hemisphere, Journal of the Atmospheric Sciences, 48, 2159–2178, https://doi.org/https://doi.org/10.1175/1520-0469(1991)048<2159:STITSH>2.0.CO;2, 1991.

Wernli, H. and Schwierz, C.: Surface Cyclones in the ERA-40 Dataset (1958-2001). Part I: Novel Identification Method and Global Climatology, Journal of the Atmospheric Sciences, 63, 2486–2507, https://doi.org/https://doi.org/10.1175/JAS3766.1, 2006.

Wernli, H. and Sprenger, M.: Identification and ERA-15 climatology of potential vorticity streamers and cutoffs near the extratropical tropopause, Journal of the Atmospheric Sciences, 64, 1569–1586, https://doi.org/10.1175/JAS3912.1, 2007.

Winters, A. C. and Martin, J. E.: The role of a polar/Subtropical jet superposition in the may 2010 Nashville flood, Weather and Forecasting, 29, 954–974, https://doi.org/10.1175/WAF-D-13-00124.1, 2014.

Woollings, T., Barnes, E., Hoskins, B., Kwon, Y. O., Lee, R. W., Li, C., Madonna, E., McGraw, M., Parker, T., Rodrigues, R., Spensberger, C., and Williams, K.: Daily to decadal modulation of jet variability, Journal of Climate, 31, 1297–1314, https://doi.org/10.1175/JCLI-D-17-0286.1, 2018.

Zhao, Y., Deng, L., Li, Z., and Wang, Y.: Quantitative Attribution of Vertical Motion Responsible for Summer Heavy Rainfall Over North China, Journal of Geophysical Research: Atmospheres, 127, https://doi.org/10.1029/2021JD035765, 2022.